Thermophysics and Aeromechanics, *2013*, *Vol. 20*, *No. 4*

Verification of the open package OpenFOAM on dam break problems

A.Zh. Zhainakov[1] and A.Y. Kurbanaliev[2]

[1]*Asanaliev Institute of Mining and Mining Technologies of the Razzakov Kyrgyz State Technical University*, *Bishkek*, *Kyrgyzstan*

[2]*Kyzyl-Kiysk Humanitarian-Pedagogic Institute of the Batken State University*, *Batken*, *Kyrgyzstan*

E-mail: kurbanaliev@rambler.ru

(*Received September 7*, *2012*; *in revised form November 21*, *2012*)

The work presents the results of mathematical modeling of large-scale flows in areas with a complex topographic relief. The Reynolds-averaged Navier—Stokes equations constitute the basis of the three-dimensional unsteady modelling. The well-known Volume of Fluid method implemented in the solver interFoam of the open package OpenFOAM 1.7.1 is used to track the free-boundary location. The mathematical model adequacy is checked by comparing with experimental data. The efficiency of the applied technology is illustrated by the example of modeling the breakthrough of the dams of the Andijan (Uzbekistan) and Papan (near the Osh town, Kyrgyzstan) reservoirs.

Key words: three-dimensional modeling, free boundary, the volume-of-fluid method, dam break, flood, OpenFOAM.

Introduction

The mathematical modeling using the advanced applied packages of computational fluid dynamics is an efficient tool for predicting various man-made and natural phenomena. The water flood of the regions and urban areas takes the first place among natural spontaneous cataclysms in terms of the repetitions, extension area, and annual material damage.

In the present paper, the problem of the prediction of consequences of a large-scale man-made disaster caused by the dam break is posed by the example of the Papan (near the Osh town, Kyrgyzstan) and Andijan (Uzbekistan) reservoirs.

The adopted mathematical model is presented in Section 1. The general technology of finding the numerical solution of the adopted mathematical model is presented in Section 2, the initial and boundary conditions, the model discretization methods are given. Section 3 contains the results of verifying the package OpenFOAM 1.7.1 by various dam break examples. Finally, the examples of using the OpenFOAM package for modeling the breaks of the dams of the Papan and Andijan reservoirs are considered in Section 4.

1. Mathematical model

The mass and momentum conservation laws for viscous incompressible liquid in the absence of mass forces lead to the following unsteady Navier—Stokes equations [1, p. 293]:

$$\partial\left(\rho\overline{u_i}\right)\Big/\partial x_i = 0, \tag{1}$$

$$\frac{\partial}{\partial t}(\rho\overline{u_i}) + \frac{\partial}{\partial x_j}(\rho\overline{u_i}\,\overline{u_j} + \rho\overline{u_i'u_j'}) = -\frac{\partial\overline{p}}{\partial x_i} + \frac{\partial\overline{\tau_{ij}}}{\partial x_j}, \tag{2}$$

where $\overline{u_i}$ are the mean velocity components, ρ is the density, $\overline{p}$ is the mean pressure, $\overline{\tau_{ij}} = \mu\left(\frac{\partial\overline{u_i}}{\partial x_j} + \frac{\partial\overline{u_j}}{\partial x_i}\right)$ is the mean tensor of viscous stresses, μ is the dynamic viscosity. The averaging is done in time, and the prime denotes the fluctuation part. In the presence of external forces, it is necessary to augment these equations by the corresponding terms.

To close the systems of equations (1), (2) it is necessary to introduce some turbulence model. Most turbulence models employed in practice are based on the concepts of turbulent viscosity and turbulent diffusion. For the flows of general form, the turbulent viscosity introduced by Boussinesq, which couples the Reynolds stresses with the mean flow gradients, may be written in the following form [1, p. 294]:

$$-\rho\overline{u_i'u_j'} = \mu_{\mathrm{t}}\left(\frac{\partial\overline{u_i}}{\partial x_j} + \frac{\partial\overline{u_j}}{\partial x_i}\right) - \frac{2}{3}\rho\delta_{ij}k.$$

The turbulence kinetic energy k and its dissipation rate ε are determined from the following transport equations [1, p. 295, 296]:

$$\frac{\partial(\rho k)}{\partial t} + \frac{\partial(\rho\overline{u_j}k)}{\partial x_j} = \frac{\partial}{\partial x_j}\left(\mu + \frac{\mu_{\mathrm{t}}}{\sigma_k}\right)\frac{\partial k}{\partial x_j} + P_k - \rho\varepsilon,$$

$$\frac{\partial(\rho\varepsilon)}{\partial t} + \frac{\partial(\rho\overline{u_j}\varepsilon)}{\partial x_j} = C_{\varepsilon 1}P_k\frac{\varepsilon}{k} - \rho C_{\varepsilon 2}\frac{\varepsilon^2}{k} + \frac{\partial}{\partial x_j}\left(\frac{\mu_{\mathrm{t}}}{\sigma_\varepsilon}\right)\frac{\partial\varepsilon}{\partial x_j},$$

where $P_k = \mu_{\mathrm{t}}\left(\frac{\partial\overline{u_i}}{\partial x_j} + \frac{\partial\overline{u_j}}{\partial x_i}\right)\frac{\partial\overline{u_i}}{\partial x_j}$ is the rate of the generation of the turbulence kinetic energy by mean flow, and $\mu_{\mathrm{t}} = \rho C_\mu\frac{k^2}{\varepsilon}$ is the turbulent viscosity.

The coefficients of the model have the following standard values: $C_\mu = 0.09$, $C_{\varepsilon 1} = 1.44$, $C_{\varepsilon 2} = 1.92$, $\sigma_k = 1.0$, $\sigma_k = 1.3$.

The method of determining the interface between two phases — water and air occupies special place at the modeling of the flow class under consideration. According to the main idea of the volume-of-fluid method [1, p. 384], one determines for each computational cell a scalar quantity, which represents the degree of filling the cell with one phase, for example, water. If this quantity is equal to 0, it is empty; if it is equal to 1, then it is filled completely. If its value lies between 0 and 1, then one can say, respectively, that this cell contains the free (interphase) boundary. In other words, the volume fraction of water α is determined as the ratio of the water volume in the cell to the total volume of the given cell. The quantity $1 - \alpha$ represents,

respectively, the volume fraction of the second phase — air in the given cell. At the initial moment of time, one specifies the distribution of the field of this quantity, and its further temporal evolution is computed as the solution of the following transport equation:

$$\frac{\partial \alpha}{\partial t} + \frac{\partial (\alpha \overline{u_i})}{\partial x_i} = 0.$$

The free boundary location is determined by the equation $\alpha(x, y, z, t) = 0$. Therefore, the physical properties of the gas-liquid mixture are determined by averaging with the corresponding weight coefficient:

$$\rho = \alpha\rho_1 + (1-\alpha)\rho_2, \quad \mu = \alpha\mu_1 + (1-\alpha)\mu_2.$$

Here the subscripts 1 and 2 refer to the liquid and gaseous phases.

The essence of the volume-of-fluid method implemented in the solver interFoam of the OpenFOAM 1.7.1 package [2] lies in the fact that the interface between two phases is not computed explicitly, but is determined, to some extent, as a property of the field of the water volume fraction. Since the volume fraction values are between 0 and 1, the interphase boundary is not determined accurately, however, it occupies some region, where a sharp interphase boundary must exist in the proximity.

2. Modelling technology

Initial conditions

It is necessary to specify for the unsteady problem the initial values of all dependent variables. The values of all velocity components are equal to zero because according to the condition of the problem under study, there is no motion until the moment of time $t = 0$. The pressure is also equal to zero. The turbulence kinetic energy and its dissipation rate have some small value, which ensures a good convergence of the numerical solution at the first integration steps. The initial distribution of the volume fraction α is non-uniform because not all the computational cells are filled with water.

Boundary conditions

The no-slip condition is specified at solid walls of the computational region, which gives the zero components of the velocity vector. The Neumann conditions are specified for the pressure and water volume fraction: $\partial p / \partial n = 0$ and $\partial \alpha / \partial n = 0$; the boundary conditions for the turbulence kinetic energy k and its dissipation rate ε were specified with the aid of the technique of wall functions [1, p. 298, 299]. The influence of surface tension forces between the solid wall and the gas-liquid mixture were not taken into account.

The zero values for the pressure, water volume fraction, and all velocity components are specified at the free boundary.

Discretization of governing equations

The discretization of the computational region is obtained by the method of control volumes [3, p. 30]. The use of an upwind difference scheme for the convective and Gauss linear scheme for diffusion terms yields an acceptable accuracy of numerical computations.

The explicit Euler first-order method was used for the discretization of the derivative with respect to time. Numerical solution of the unsteady equations coupled via the pressure was based on the PISO method [1, p. 176] with the number of correctors equal to 3.

The iterative solvers PCG and PBiCG — the preconditioned conjugate gradient and preconditioned biconjugate gradient methods were used for solving the obtained system of linear

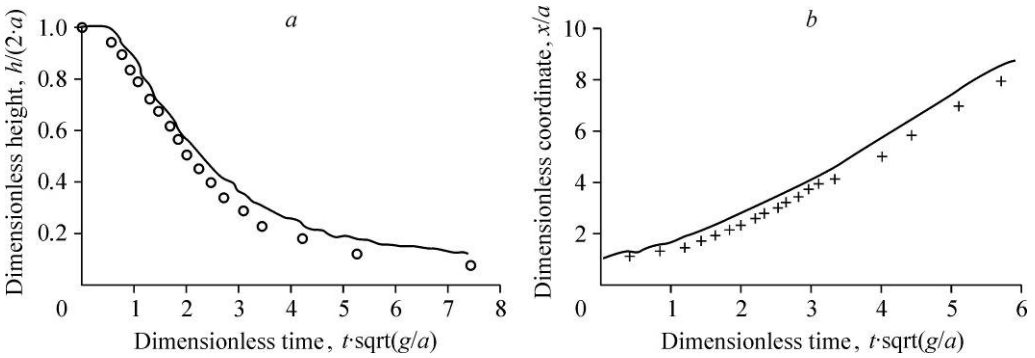

Fig. 1. Comparison of numerical and experimental data.
a — water column height change, *b* — the flow leading front position.

algebraic equations. The procedures based on a simplified Cholesky's incomplete factorization scheme DIC and on the simplified incomplete LU factorization DILU were used as preconditioners.

More detailed information about the boundary and initial conditions, discretization techniques, and the solution of systems of algebraic equations may be found in the work [2].

3. The OpenFOAM package verification

The problem on the liquid column collapse in a horizontal duct of rectangular cross section [4] is the first test problem. At the initial moment of time, the rectangular column of a viscous incompressible fluid is at rest. The column starts collapsing under the gravity force.

The numerical results (solid line) are compared with experimental data (markers) of the work [4] in Fig. 1, where $a = 0.05715$ m is the water column width in the x-axis direction, $g = 9.81$ m/s^2 is the free-fall acceleration. The agreement between experiment and numerical computation is to be recognized as acceptable.

Figure 2 shows the configuration of the next model problem. The model represents a reservoir of hexahedral shape whose length is 3.22 m, height 2 m, and width 1 m [5]. The water column of height $H = 0.6$ m, length 1.2 m, and width 1 m lies in the left lower corner. To measure the pressure force of fluid flow on the right reservoir wall the corresponding pressure probe was placed at point P with coordinates $x = 3.22$ m and $y = 0.16$ m. Besides, the levels h_1 and $h_2$of the water free surface were measured in two sections at $x_1 = 2.725$ m and $x_2 = 2.228$ m. The density of water was equal to 998.2 kg/m^3, and that of air was equal to 1.225 kg/m^3. Despite the fact

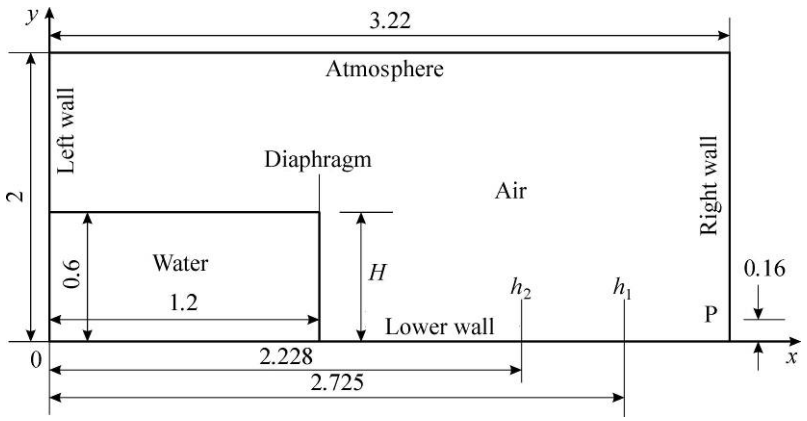

Fig. 2. Test problem configuration.

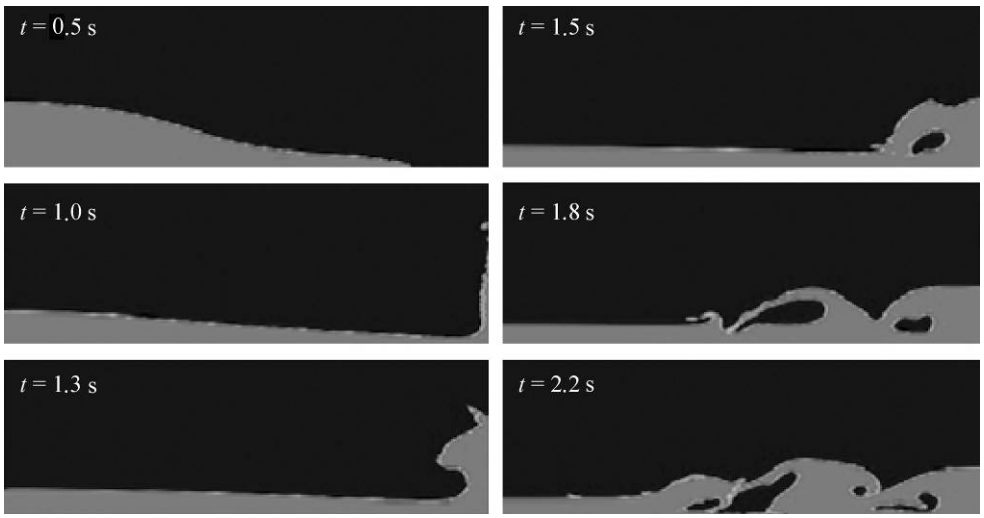

Fig. 3. Water column motion at different moments of time.

that the experiment was three-dimensional, the configuration simplicity has enabled its modeling in the two-dimensional approximation. The total duration of modeling in time amounted to 2.5 s.

Figure 3 shows the numerical results for different moments of time.

The diaphragm is suddenly removed at the moment of time $t = 0$, and the water column runs under the gravity force into the right empty part of the reservoir. At the moment of time $t \approx 0.65$ s, the water reaches the right wall and, impinging on it under the inertia force, moves upwards. The flow is thinned as it moves upwards along the right wall, and at the moment of time $t = 1.3$ s, when the gravity force exceeds the inertia force, there occurs a reverse flow of water with the formation of a typical bend of its surface. The reverse wave formed in such a way reaches the main flow, impinges onto it, and forms the secondary wave, etc. (at $t = 1.5$ s and $t = 1.8$ s). After the moment of time $t = 2.2$ s, the water inertia drops significantly, and the further consideration of the motion is of no practical interest.

Figure 4 shows the numerical (solid line) and corresponding experimental (markers) data on the water column height in sections with coordinates $x_1 = 2.725$ m and $x_2 = 2.228$ m. The coincidence between these data is satisfactory up to the moment of time $t \approx 1.5$ s for section $x_1 = 2.725$ m (Fig. 4*a*).

After this moment of time, the reverse wave moving oppositely to the main stream impinges onto the free surface, and this give rise to certain inaccuracies both in numerical and experimental data. The inaccuracies of such a kind were also observed in the work [6], where the well-known commercial package FLUENT was used for numerical modelling. The results of this work are presented in Fig. 5 in a form similar to Fig. 4. The water column height (h_1, h_2)

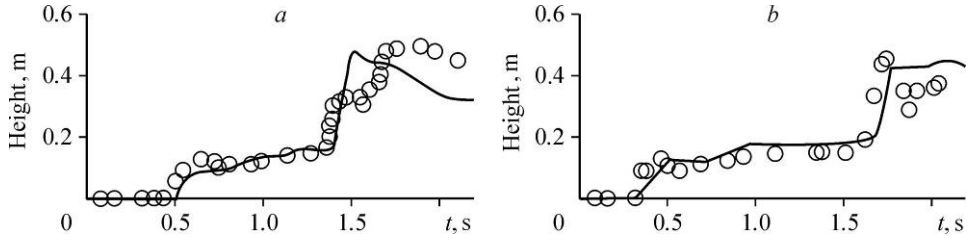

Fig. 4. Water column height in different sections.
$x_1 = 2.725$ m (*a*) and $x_2 = 2.228$ m (*b*).

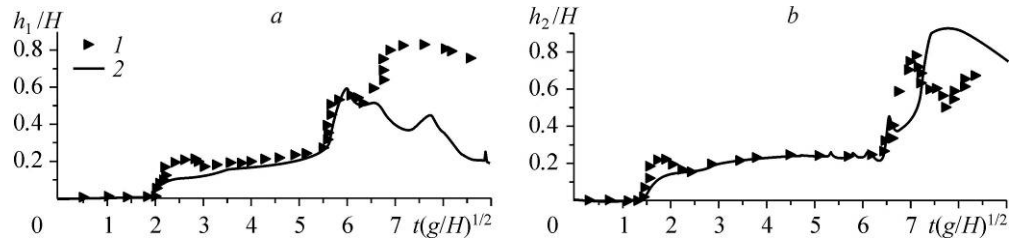

Fig. 5. Water column height from the work [6] at $x = 2.725$ m (*a*) and 2.228 m (*b*).
1 — experiment, *2* — computation of the work [6].

has been nondimensionalized here by quantity H, and the time is presented in the dimensionless form $\tau = t(g/H)^{0.5}$, where t is the physical time, $g = 9.81$ m/s^2 is the free-fall acceleration, $H = 0.6$ m is the initial water column height. One can conclude from a comparison of Figs. 4 and 5 that the free surface levels in two different sections have been predicted more accurately in the present work.

The task of determining the pressure P on the obstacle is very important at the solution of unsteady problems with free surface, in particular, at the interaction of forming waves with various obstacles. Figure 6 shows the numerical results (solid line) for the pressure of the fluid on the right wall at point P with coordinates ($x = 3.2$ m, $y = 0.16$ m) and the corresponding experimental data (markers). The exact pressure value at point P cannot be measured because the pressure probes have a finite size — a circle about 90 mm in diameter.

The numerical pressure at the pressure probe center (see Fig. 6*a*) increases slowly with time, after the moment of time $t = 1.5$ s or after the second maximum the coincidence of experimental data with numerical results improves. The character of the numerical pressure at the lower point of the probe (see Fig. 6*b*) agrees fairly well with the character of the variation of corresponding experimental data, however, the maximum values are slightly underestimated.

It is assumed at the numerical modeling that the diaphragm is removed suddenly that is its vertical velocity is infinite. On the other hand, there can be also different physical conditions, which are hard to take into account at the numerical modeling. A detailed analysis of the conditions for conducting the experiment shows that this velocity has a finite value. The verification experimental data under the same conditions give different results, which do not coincide with one another [5]. In addition, the above discrepancies between the computation and experiment after the moment of time $t = 1.5$ s can probably be explained by the two-dimensionality of the employed model. It is possible that the flow acquires a three-dimensional character at some points of the computational region.

Comparing the data of the present work (Fig. 4) and the work [6] (Fig. 5) one can assert that the numerical results of modeling the task under consideration, which were obtained with the aid of the open package OpenFOAM, are closer to the experimental data than the results obtained with the aid of the commercial package FLUENT.

The problem of the fluid column breakdown in a reservoir of rectangular shape with an obstacle [7] is the next, more complex test problem. The chosen coordinate system and the problem diagram without the geometric proportion preservation are shown in Fig. 7.

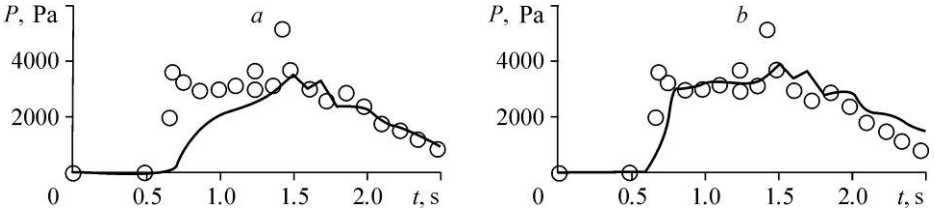

Fig. 6. Pressure variation at point P.
Pressure at the center (*a*) and at the lower point (*b*) of the probe.

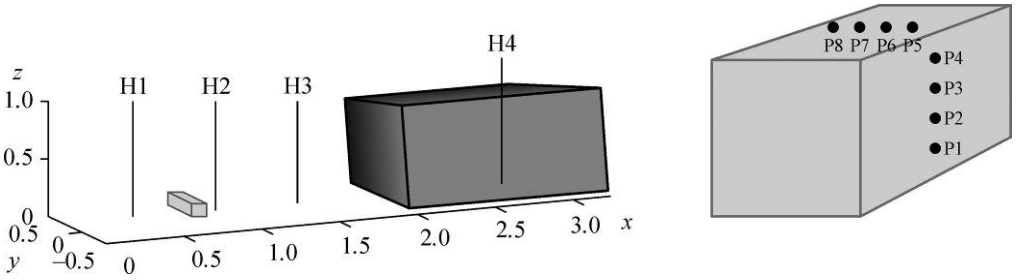

Fig. 7. Configuration (on the left) and location of measurement pressure probes (on the right).

An open reservoir 3.22 m in length with cross section of 1×1 m^2 has been used in experiment. The reservoir was initially partitioned into two unequal parts by a vertical wall located in section $x = 2$ m. The water 0.55 m in height is located behind this wall, another reservoir part is empty. A container 40 cm in length with cross section of 16×16 cm^2 is located in this reservoir part. The container left-face coordinate equals $x = 0.67$ m.

At the execution of experiment, the water column height and the fluid pressure on the container surface were measured. The location of measuring probes is shown in Fig. 8. Four probes were used to measure the water column height: the one on the part filled with water — H4, and the remaining ones H1, H2, and H3 were located in the reservoir empty part. The coordinates of these probes are $x = 0.5$, 1.0, 1.5, and 2.66 m, respectively.

The container was supplied with eight pressure probes: four probes on the exterior surface at points with coordinates $z = 0.025$, 0.063, 0.099, and 0.136 m, and the remaining four probes were located on the container upper side with coordinates $x = 0.806$, 0.769, 0.733, and 0.696 m. The probes on the exterior surface were located at the distance of 0.026 m to the left of the central line ($y = 0$), and the probes on the upper surface were located at the distance of 0.026 m of this line. The force exerted on the container on the water stream side was also measured in experiment.

The water was at rest up to the moment of time $t = 0$. At the moment of time $t = 0$, the separating wall was removed suddenly, and the water column ran into the reservoir empty part under the gravity force. The 180×60×80 computational grid was used, and the CPU time amounted to 6 s. The initial time step was 0.001 s, and it was varied further depending on the Courant number, which was equal to 0.85.

Figures 8 and 9 show the comparison of numerical and experimental data for the moments of time $t = 0.4$ and 0.6 s, respectively. The pictures of shooting done during the experiment

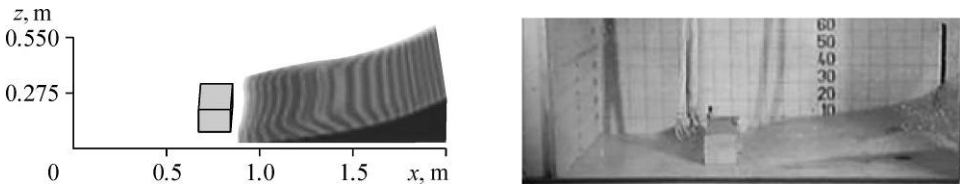

Fig. 8. Comparison of numerical (on the left) and experimental data (on the right) at the moment of time $t = 0.4$ s.

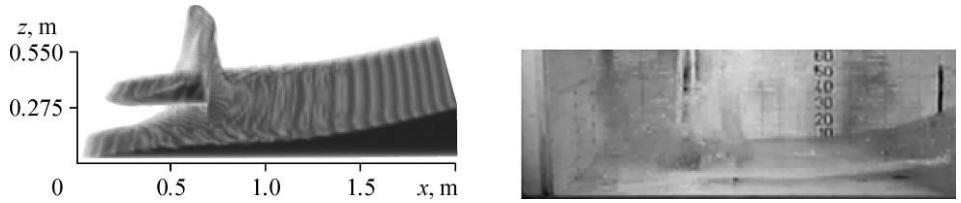

Fig. 9. Comparison of numerical (left) and experimental (right) data at the moment of time $t = 0.6$ s.

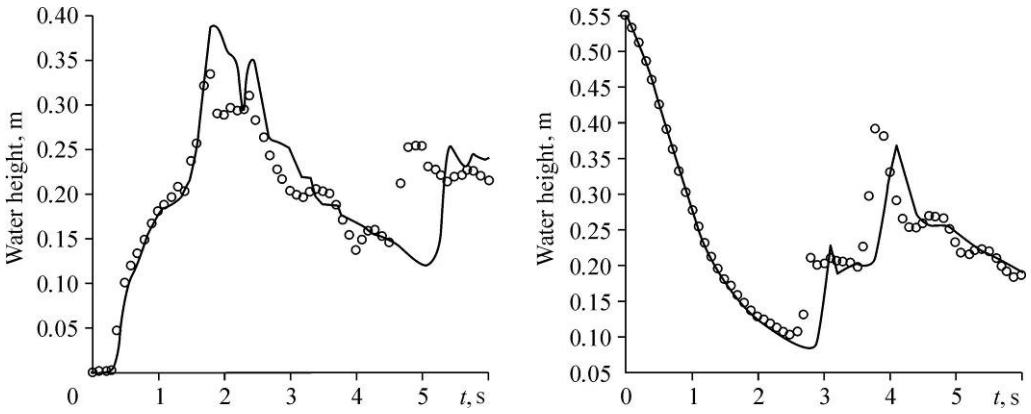

Fig. 10. Water flow heights at points H2 (left) and H4 (right).

are shown on the right. One can notice a fairly good visual coincidence of the numerical results with experimental data.

The time of reaching the container by water flow both in experiment and at the numerical simulation is the same. Besides, the free surface shapes forming after the flow impact onto the container also coincide. One can note, however, that there are at the numerical modeling some imperfections of the free surface between water and the ambient medium — air.

Figure 10 shows the water flow height at two different points: in the reservoir and in the immediate proximity of the container. There is a fairly good agreement between them until the water returns from the back wall after the moment of time $t \approx 1.8$ s. After that, the numerical data (solid lines) prove to be somewhat higher than the experimental ones (markers). At the moment of time of ≈ 5 s, the secondary wave reaches the neighborhood of the probe *H*2. This time is, however, equal to about 5.3 s at the numerical modeling. The general character of the variations of the numerical and experimental data nevertheless coincides.

Figure 11 shows the moment of time $t = 0.5$ s when the wave reaches the container has been predicted with a good accuracy, however, the computed pressure value (solid lines) is slightly overestimated as compared to the experimental value (markers) (the left figure). The numerical values of the second pressure maximum at point P2 are, however, shifted in comparison with experiment to the right by 0.6 s, and at point P7, they are shifted by 0.5 s. As the experiment has shown, the moment of time when the flow reaches repeatedly the container (≈ 4.7 s) is seen in these figures fairly well. Besides, when comparing the numerical and experimental pressure values at points P7 (the right figure) one can notice some differences. After $t = 1.3$ s,

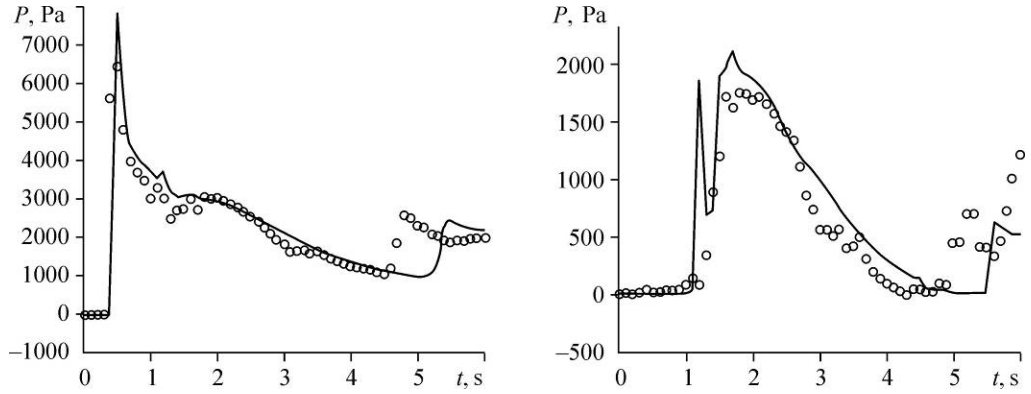

Fig. 11. Pressure at points P2 (left) and P7 (right).

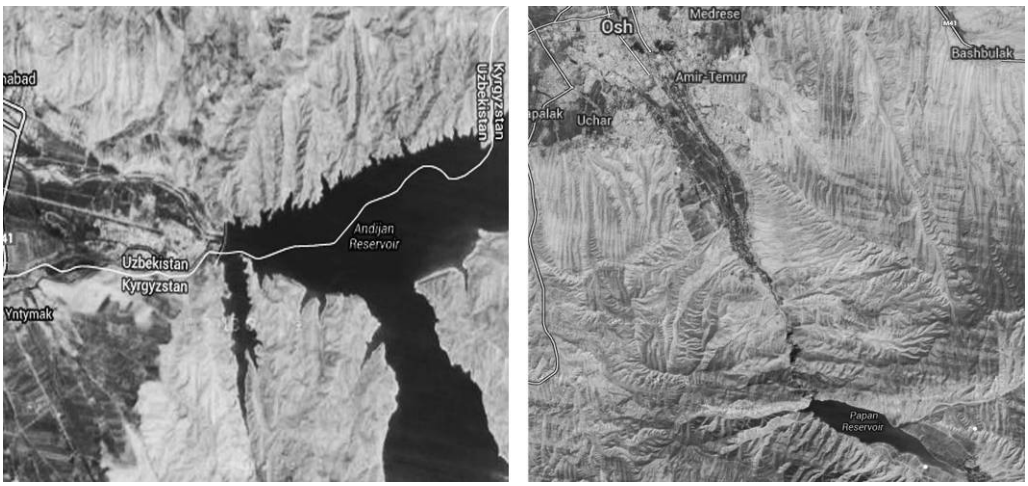

Fig. 12. Maps of the Andijan (left) and Papan (right) reservoirs.

a small oscillation lasting for about 0.2 s takes place in numerical computations, which is not observed in experiment.

4. Flow modeling in real region

To illustrate the techniques of the application of numerical modeling of large-scale hydrodynamic computations we consider the problem of computing the flood process in the areas near the dams of the Andijan and the Papan reservoirs (see Fig. 12). It is to be emphasized here that the situation of a real breakthrough of the dam and the flood of the areas at the lower level is not modeled here but the fundamental possibility of using the above technology under the availability of necessary topography data is demonstrated. The topography data of Digital Terrain Elevation Data [8] were used in computations, which were converted subsequently into the stl format. The hexahedral background grid generated with the aid of the utilities blockMesh and snappyHexMesh of the OpenFOAM package was transformed into a three-dimensional surface, which is employed for modeling the flood process (Fig. 13). The computations were done in the both cases on computer Pentium®Dual-Core CPU T4400@2.20 GHz, 2.87 Gb RAM.

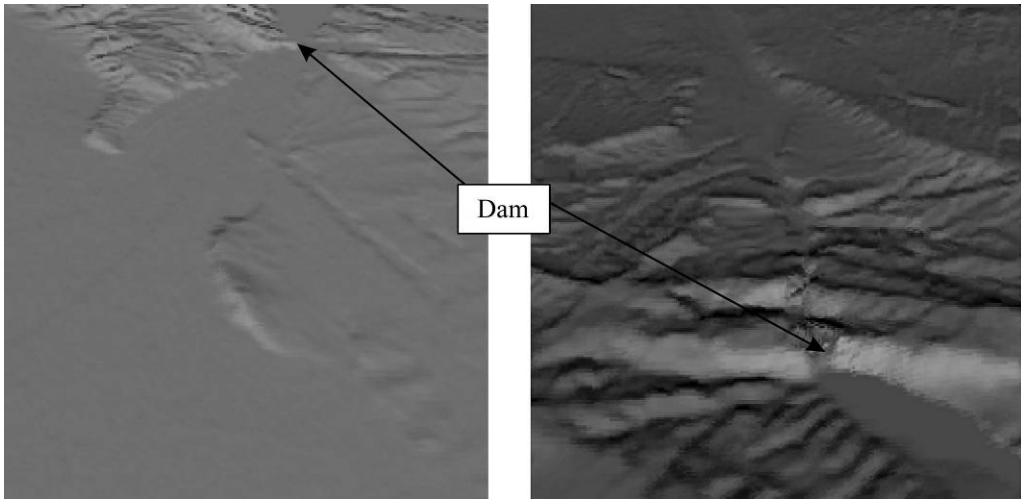

Fig. 13. Three-dimensional surface of the Andijan (left) and Papan (right) reservoirs areas.

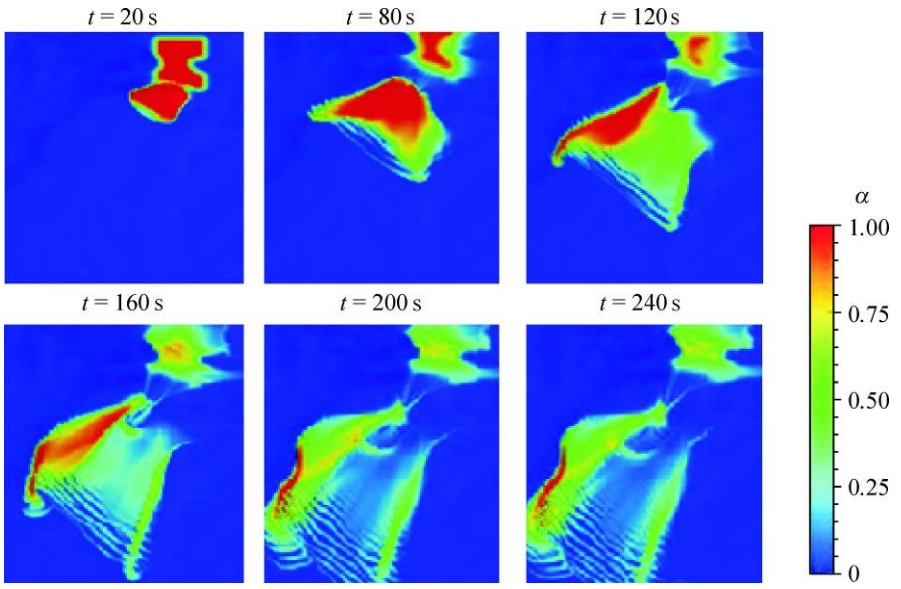

Fig. 14. Flow pattern for the Andijan reservoir.

For the Andijan reservoir, the computational field had the sizes 6000×4000×1500 m, the physical modeling time amounted to about nine hours for the 120×120×80 grid. Figures 14 and 15 show different stages of the flood in areas with real topology. The red color corresponds to a pure water flow, and the blue color corresponds to air flow (there is no water flow in blue regions). It is seen in Fig. 14 that the leading front of water flow reaches during 240 s the lower boundary of the computational region passing a distance of about 6000 m, covers the most part of the area located downstream.

The computational field for the Papan reservoir has the sizes 5000×5000×1300 m (Fig. 15).

The total computing time in the case of the 50×60×30 grid amounts to about 5 hours. As is seen in Fig. 15, after the moment of time $t \approx 200$ s there forms a reverse flow (Figs. 15*d* and 15*c*), and after the moment of time $t = 260$ s, it separates into two parts — one part is

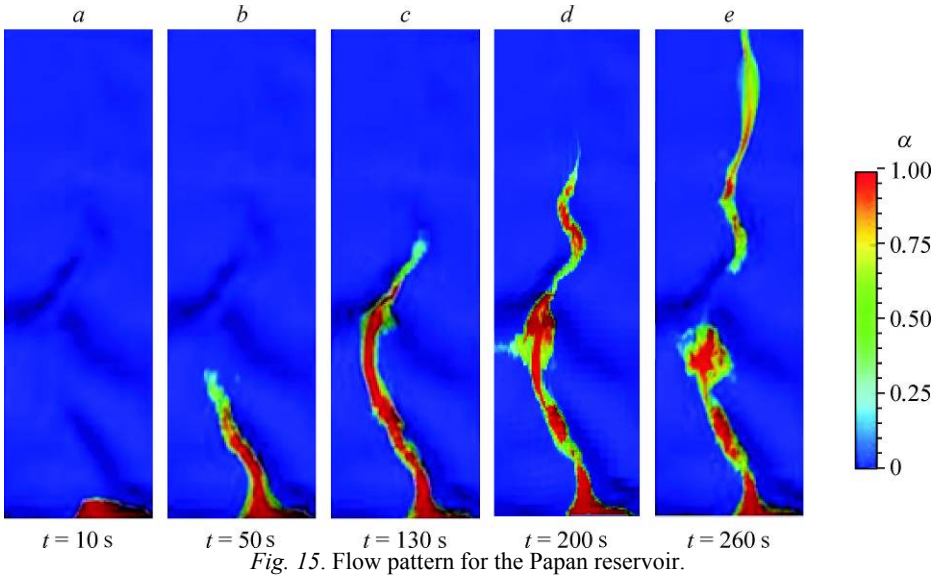

Fig. 15. Flow pattern for the Papan reservoir.

in the zone of reverse flows, and the other continues its flow in the lower part of the river bed. The computations show that about 60 % of the entire initial water volume remains in the zone of reverse flows.

The present work does not account for the interaction of water flow with river-bed flora and various structures, which change significantly the general flow pattern leading to a flood zone increase.

It is necessary to note specially that due to the limitations of the computer computational resources the computing mesh size was chosen relatively crude. Therefore, one must consider the presented computational results as the estimation ones, they need verification on a finer mesh.

Conclusions

The results of the mathematical modeling of complex hydrodynamic phenomena on the basis of unsteady three-dimensional Navier—Stokes equations describing the dynamics of a gas-liquid mixture with free boundary have been presented. The adequacy of the employed model has been verified by the example of the classical problems of computational fluid dynamics. Special attention has been paid to the accuracy of the computation of the water flow level and the gas-liquid flow pressure on the reservoir walls. The efficiency of the employed technology has been illustrated by the example of modeling the breaks of the dams of the Andijan (Uzbekistan) and Papan (near the Osh town, Kyrgyzstan) reservoirs. The developed technology is universal and can be used for the flood modeling for a real relief. It is shown that the relief features are a substantial factor.

The work was done within the framework of the Fulbright Foreign Research Scholarship program of the U.S. State Department jointly with Professor Greg Olyphant from the Indiana University, Bloomington, USA.

References

1. J.H. Ferziger and M. Peric, Computational Methods for Fluid Dynamics, Springer Verlag, Berlin, 2002.

2. Modified by OpenFOAM Foundation, OpenFOAM®V1.7.1 Documentation, 2011–2013, [Electronic resource], Mode access: http://www.openfoam.org/archive/1.7.1/docs/.

3. S.V. Patankar, Numerical Heat Transfer and Fluid Flow, Hemisphere Publ. Corp., New York, 1980.

4. J.C. Martin and W.J. Moyce, An experimental study of the collapse of liquid columns on a rigid horizontal plane, Phil. Trans. Royal Soc, London, Series A, Math. and Physical Sci., 1952, Vol. 244, No. 882, P. 312–324.

5. Z.Q. Zhou, J.O.D. Kat, and B. Buchner, A nonlinear 3D approach to simulate green water dynamics on deck, in: 7th Int. Conf. on Numerical Ship Hydrodynamics, Nantes, France, 1999, P. 5.1-1–5.1-15.

6. K. Abdolmaleki, K.P. Thiagarajan, and M.T. Morris–Thomas, Simulation of the dam break problem and impact flows using a Navier—Stokes solver, in: 15th Australasian Fluid Mechanics Conf., University of Sydney, Australia, 13–17 December 2004, P. 135–138.

7. K.M.T. Kleefsman, G. Fekken, A.E.P. Veldman, B. Iwanowski, and B. Buchner, A Volume-of-fluid based simulation method for wave impact problems, J. Comput. Phys., 2005, Vol. 206, No. 1, P. 363–393.

8. Digital Terrain Elevation Data (DTED), 2012, [Electronic resource], Mode access: http: // data.geocomm.com/ catalog/KG/group121.html.